Advance Sustainable Science, Engineering and Technology (ASSET)
Vol. 7, No.4, October 2025, pp. 02504023-01 ~ 02504023-017
ISSN: 2715-4211 DOI: https://doi.org/10.26877/asset.v7i4.2613

Physics-Informed Neural Network with Thevenin Equivalent Circuit for Accurate SOC Li-ion Battery Estimation

Chico Hermanu Brillianto Apribowo[1*], Muhamad Dzaky Ashidqi[1,2], Zainal Arifin[3], Henry Probo Santoso[4]

[1]Department of Electrical Engineering, Universitas Sebelas Maret, Jl. Ir. Sutami 36 A, Kentingan, Jebres, Surakarta 57126, Central Java, Indonesia

[2]Department of Electrical Engineering, Universitas Sains Indonesia, Jl. Akses Tol Gandasari, Cikarang Barat, Bekasi 17530, West Java, Indonesia

[3]Department of Mechanical Engineering, Universitas Sebelas Maret, Surakarta, Jl. Ir. Sutami 36 A, Kentingan, Jebres, Surakarta 57126, Central Java, Indonesia

[4]Department of Engineering and Design, University of Sussex, Falmer Brighton, BN1 9RH, United Kingdom.

*chico @ staff.uns.ac.id

Abstract. Accurate state of charge (SOC) estimation is essential for the safety, performance, and longevity of lithium-ion batteries. Physics-based models such as equivalent circuit models (ECMs) are computationally efficient but struggle under nonlinear and time-varying conditions, whereas purely data-driven approaches often lack interpretability. This study proposes a hybrid framework that integrates a physics-informed neural network (PINN) with a first-order Thevenin ECM for dynamic SOC estimation using only terminal voltage and current inputs. The method incorporates physically derived parameters including open-circuit voltage (OCV), polarization resistance, and capacitance identified through pulse testing. An eighth-order OCV–SOC polynomial regression optimized with a genetic algorithm (GA) enables nonlinear mapping, while the Newton–Raphson (NR) method is applied for final SOC estimation. Experimental validation was performed on 18 Ah lithium iron phosphate (LFP) cells over 300 charge–discharge cycles at 20 °C, extended up to 2000 cycles under 1C/2C rates with cut-off voltages of 3.7 V and 2.7 V. Comparative analysis with extended kalman filters (EKF) and standard neural networks (NN) demonstrates the superiority of the proposed method, achieving a root mean squared error (RMSE) of 0.103, mean absolute percentage error (MAPE) of 0.702%, and coefficient of determination (R^2) of 0.998. By embedding physical constraints into the learning process, the PINN enhances accuracy, robustness, and generalizability, while reducing estimation uncertainty, thereby offering a scalable and interpretable solution for real-time battery management systems (BMS) in electric vehicles (EVs) and battery energy storage systems (BESS).

Keywords: battery management systems (BMS), energy storage systems (ESS), equivalent circuit model (ECM), hybrid modeling, state of charge (SOC), uncertainty quantification

(Received 2025-08-22, Revised 2025-09-15, Accepted 2025-09-23, Available Online by 2025-09-25)

1. Introduction

The growing use of lithium-ion batteries in BESS necessitates precise models to estimate battery states like state of charge (SOC). SOC, a key operational parameter, indicates the remaining battery energy and is crucial for managing energy, ensuring safety, and optimizing performance [1]. Estimating SOC in real-world scenarios is challenging due to the dynamic, nonlinear battery behavior affected by electrical, thermal, and aging factors [2-3]. These complexities have motivated diverse approaches to SOC estimation that can broadly be categorized into physics-based, data-driven, and hybrid frameworks.

Electrochemical models and equivalent circuit models (ECMs) are the most established physics-based approaches. Electrochemical models provide high fidelity by explicitly representing reaction kinetics, ion transport, and diffusion processes inside the cell [4–5]. Their interpretability and accuracy are strong advantages, but their reliance on numerous hard-to-measure parameters and high computational demand restricts their practical use in embedded and real-time systems [6]. In contrast, ECMs such as the Thevenin and partnership for a new generation of vehicles (PNGV) models approximate cell dynamics with resistors, capacitors, and voltage sources, striking a balance between simplicity and predictive ability [7–11]. ECMs are widely used because of their ease of parameterization and compatibility with onboard battery management systems. Yet, they struggle with long-term nonlinear effects such as hysteresis, temperature sensitivity, and degradation [12].

Model-based estimation techniques have been introduced to extend ECM applicability under uncertain operating conditions. The kalman filter (KF) and its extensions remain widely adopted. The extended kalman filter (EKF) improves performance in nonlinear settings through local linearization, while the unscented kalman filter (UKF) addresses linearization errors by propagating sigma points [13–18]. Particle filters (PF) further generalize to non-Gaussian distributions using sequential monte carlo (MC) techniques [19]. These methods are robust under moderate dynamics and measurement noise. However, their performance is highly sensitive to initialization and model assumptions. For example, the EKF introduces linearization errors when nonlinearities are pronounced, while PFs require significant computational resources and can diverge if resampling strategies are inadequate [17,19,20]. Thus, while physics-based approaches provide interpretability, their accuracy degrades under highly dynamic conditions or when physical parameters shift due to aging.

Advances in machine learning (ML) and deep learning have introduced purely data-driven alternatives for SOC estimation. Classical ML methods such as decision tree, random forest (RF) and extreme gradient boosting (XGBoost) have proven effective at modeling nonlinear input–output relationships based on current, voltage, and temperature features [21–23]. These ensemble approaches mitigate overfitting and are relatively robust for static or semi-dynamic operation. However, they lack the ability to capture sequential dependencies intrinsic to battery cycling [24].

Deep learning methods, including convolutional neural network (CNN) and recurrent neural network such as long short-term memory (LSTM) have addressed this limitation by modeling temporal features [25–29]. CNNs extract localized patterns such as transient responses, while LSTMs capture long-term temporal dependencies and well suited for dynamic charge–discharge cycles. Nevertheless, these models require vast labeled datasets, are computationally intensive, and operate as black-box systems, limiting physical interpretability and raising concerns about generalization to unseen conditions [30–31].

Probabilistic data-driven methods, such as gaussian process regression (GPR), have been proposed to enhance safety by quantifying predictive uncertainty [32]. While they provide valuable insights into estimation confidence, their scalability to large datasets and high sampling rates is limited, restricting real-time use. In general, data-driven methods excel in adaptability but remain constrained by their dependence on large-scale training data and their lack of physical consistency [33–35].

To reconcile the trade-offs between interpretability and adaptability, hybrid approaches have been developed by embedding physical knowledge into data-driven models. These frameworks leverage the simplicity of ECMs while exploiting the pattern-recognition strength of neural networks [36]. Previous studies combining ECMs with shallow neural networks have shown improved accuracy over standalone approaches, but often at the cost of increased sensor requirements or limited ability to generalize under

varying conditions [37–38]. Physics-informed machine learning pipelines have further advanced the field by constraining model training with electrochemical or circuit dynamics, thereby improving physical consistency and robustness [39].

Recent progress includes embedding ECM dynamics directly into differential equation-informed neural networks (DENNs) or augmenting ECMs with machine learning to improve SOC estimation accuracy [40–42]. While these models represent an important step toward interpretable and accurate estimation, they often require multiple features beyond current and voltage, or involve complex parameter tuning that hinders practical deployment. A persistent challenge remains in designing hybrid methods that achieve high accuracy, robustness, and generalizability under dynamic conditions, while keeping sensor requirements minimal for real-time systems.

In summary, physics-based models are interpretable but limited under uncertain conditions, while data-driven models are flexible but often opaque and data-hungry. Hybrid approaches provide a promising balance, but existing works have yet to deliver a framework that simultaneously (i) embeds ECM parameters into a neural learning process, (ii) requires only essential measurements such as terminal voltage and current, and (iii) remains computationally efficient for real-time operation.

This study addresses this gap by proposing a physics-informed neural network (PINN) integrated with a first-order Thevenin equivalent circuit for dynamic SOC estimation. The objectives are: (i) to design a hybrid estimation framework that combines physically derived parameters with neural network learning, (ii) to validate its performance experimentally under dynamic load and extended cycling conditions, and (iii) to benchmark the approach against widely used estimators, including EKF and pure NN models. The novelty lies in embedding physical constraints directly into loss function of NN, thereby improving interpretability, robustness, and accuracy while reducing estimation uncertainty. This contribution offers scalable and practical solution for real-time battery management in electric vehicles and energy storage applications.

Table 1. Literature review on SOC Estimation approaches

Method	**Approach Type**	**Model Type**	**Strengths**	**Limitations**
Electrochemical Model [4-5]	Physics-Based	Electrochemical Equations	High accuracy; physically interpretable	High computational cost; requires precise parameters
Electrical ECMs [8-11]	Physics-Based	RC Networks (e.g., Thevenin, PNGV)	Real-time compatible; easy to parameterize	Inaccurate for nonlinear or longterm behavior
KF [13]	Model-Based	Statistical Estimation	Effective for linear systems; efficient	not optimal for nonlinear dynamics
EKF [16]	Model-Based	Linearized Estimation	Handles moderate nonlinearity; widely adopted	Suffers from linearization errors
UKF [18]	Model-Based	Nonlinear Estimation	Accurate without linearization	Higher computational demand
PF [19]	Model-Based	Monte Carlo Bayesian (MCB)	Works for nonlinear, non-Gaussian systems	Computationally expensive
RF [22]	Data-Driven	Ensemble Learning	Robust, interpretable	Limited temporal modeling
XGBoost [23]	Data-Driven	Boosted Trees	High accuracy; fast training	Lacks time-sequence modeling

CNN [26]	Data-Driven	Deep Learning	Learns short-term patterns	Poor for longterm dependencies
LSTM [28]	Data-Driven	RNN	Captures long-term trends	Requires large data; low interpretability
GPR [32]	Data-Driven	Probabilistic Regression	Predictive uncertainty; good accuracy	Poor scalability
Hybrid ECM - ANN [38]	Hybrid	Physical - ML	Balanced accuracy and interpretability	Unable to interpret dynamic patterns of the battery
Proposed Method	Hybrid	Physics-Informed NN	Accurate, interpretable; needs only V, I	Needs physical parameters; training complexity

2. Methods

The overall process conducted in this research to develop SOC estimation algorithm is as illustrated in the flowchart in Fig. 1 below.

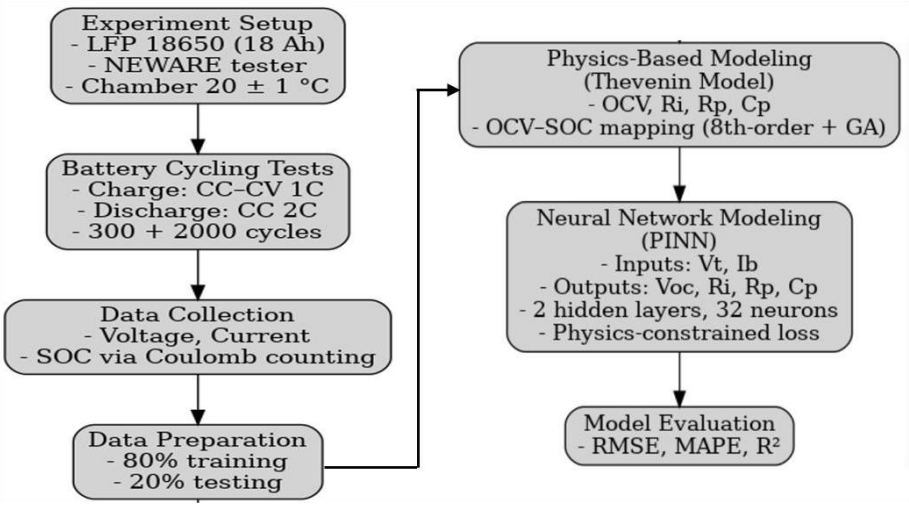

Figure 1. Research flow framework

2.1. Experiment and Data Preparation

Constructing a NN model requires a dataset with key battery parameters, notably terminal voltage and current. To achieve this, controlled experiments were conducted on lithium iron phosphate ($LiFePO_4$, LFP) 18650 cells with a nominal capacity of 18 Ah, developed by the Lithium Battery Research and Technology Centre, Universitas Sebelas Maret, Indonesia. These cylindrical cells were designed for high-power applications, capable of continuous charge and discharge at elevated current rates. Experiments were performed in a chamber with temperature maintained at 20 ± 1 °C to ensure stable ambient conditions.

The battery cycle comprised two main stages: charging and discharging. During charging, the cell was charged in constant current (CC) mode with 1C rate until the target voltage was achieved, then maintained at constant voltage (CV) until the current reduced to zero. In the discharging phase, cell was discharged in CC mode with 2C discharging rate until the voltage cut-off limit was reached. This cycle was repeated 300 times, with a 20-minute rest between cycles. Data collected included

charging/discharging current, terminal voltage, cycle count, and SOC or capacity that was calculated using coulomb counting method.

The experimental materials and equipment employed in this study consisted of:

- LFP 18650 cells supplied by the UNS Lithium Battery Research and Technology Excellence Centre,
- a NEWARE battery testing unit, and
- NEWARE data acquisition software.

These equipment and materials are illustrated in Fig. 2.

In addition, extended cycling tests were carried out for up to 2000 consecutive charge–discharge cycles without resting intervals, applying a constant current protocol. The cut-off voltages were set at 3.7 V for charging and 2.7 V for discharging. The cycling rates were established at 2C for discharge and 1C for charge, where 1C corresponds to current rate necessary to fully discharge or charge the cell within one hour.

The primary objective of these experiments was to generate a comprehensive dataset that captures the battery dynamic behavior under repeated charge–discharge cycles. Key parameters, including terminal voltage, current, and capacity, were systematically recorded to reflect both short-term dynamics and long-term degradation pattern. This dataset will be used for training and validating the proposed neural network framework. To minimize sampling bias and ensure representative coverage of the operating conditions, the collected data was randomly partitioned into two subsets. A total of 80% of the samples were allocated for training the PINN enabling the model to learn the underlying relation between voltage, current and SOC. The remaining 20% was reserved exclusively for independent testing and validation, ensuring that model performance was assessed on unseen data. This randomized splitting strategy improves the robustness of the evaluation and enhances the generalizability of the proposed method across varying cycling conditions.

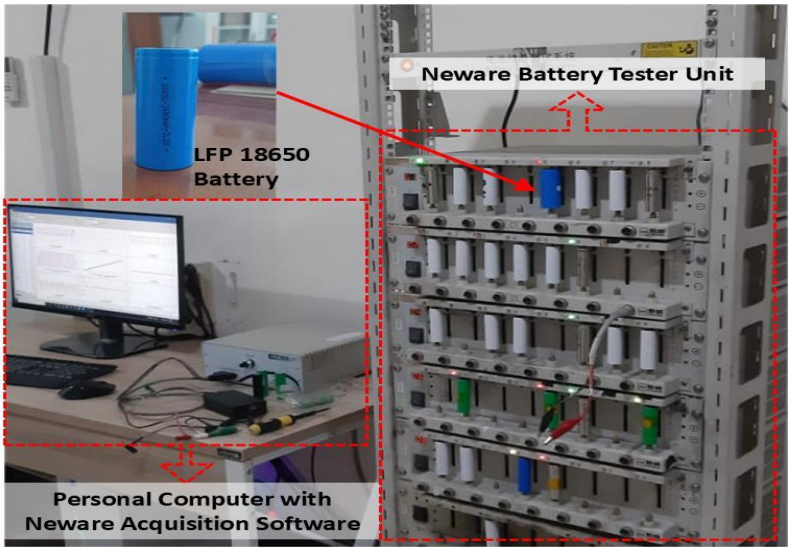

Figure 2. Experiment tools and materials

2.2. ECM modeling

In this work, a Thevenin equivalent circuit model (first-order) was adopted due to the simplicity and satisfactory accuracy. The model represents the electrical behavior of the battery by combining an open-circuit voltage (OCV) source in series with a resistor (internal resistance) and a parallel resistor and capacitor (R-C) network, as illustrated in Fig. 3.

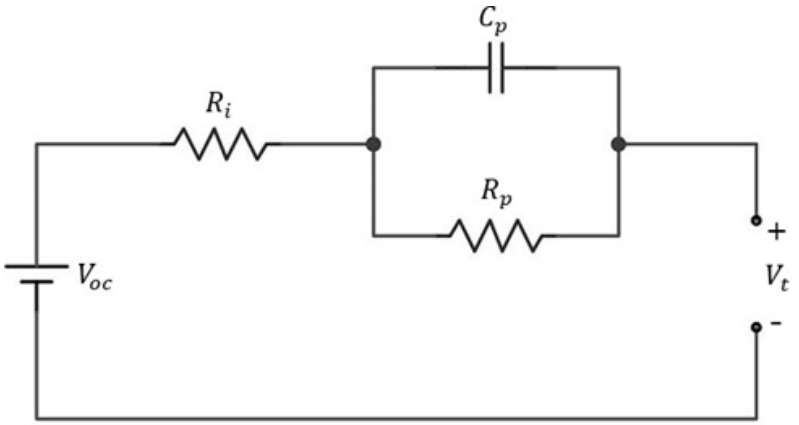

Figure 3. The first-order thevenin equivalent circuit model

V_t is terminal voltage of the battery that can be expressed mathematically as:

$$V_t = V_{oc} - I_b.R_i - V_{RC} \tag{1}$$

V_{oc} is open circuit voltage, I_b is current accross the battery, R_i is internal resistance, and V_{RC} is the voltage in the R-C branch. The R-C branch is modeled as a parallel network consist of a resistor and a capacitor. The voltage V_{RC} across this branch follows a first-order differential equation:

$$\frac{dV_{RC}(t)}{dt} = \frac{I_b(t)}{C_p(t)} - \frac{V_{RC}(t)}{R_p(t).C_p(t)} \tag{2}$$

R_p and C_p are the resistance and capacitance in the parallel R-C branch. For modeling implementation, this form is discretized with sampling time 1 s. The discretized RC model is:

$$V_{RC}(k+1) = e^{-\Delta t\left(\frac{1}{R_P C_P}\right)} V_{RC}(k) + R_p\left(1 - e^{-\Delta t\left(\frac{1}{R_P C_P}\right)}\right) I_b(k) \tag{3}$$

In SOC estimation, the parameters V_{oc}, R_p, and C_p are vital. They can vary with temperature, current rate, and battery health. When accurately identified, these parameters effectively represent the battery's internal behavior and allow precise SOC tracking.

2.3. OCV-SOC Mapping

The OCV dynamic from the ECM aids in real-time and online SOC estimation. The derived V_{oc} is related to SOC through an 8th-order polynomial regression. This approach is popular for its adaptability in fitting the OCV–SOC curve, particularly for Li-ion batteries like LFP or NMC. As detailed in (4), the polynomial fitting uses estimated OCV values.

$$V_{OC}(SOC) = \alpha_0 + \alpha_1 SOC + \alpha_2 SOC^2 + \alpha_3 SOC^3 + \cdots + \alpha_8 SOC^8 \tag{4}$$

$\alpha_0, \alpha_1, \ldots, \alpha_8$ are the polynomial coefficients obtained through least squares fitting. Higher-order fitting is often required for $LiFePO_4$ and NMC chemistries because their OCV–SOC curves exhibit nonlinear plateaus and inflection points that cannot be captured accurately with low-order polynomials. In this study, orders from 4 to 8 were tested, and while 4th- and 6th-order regressions showed larger residuals near the flat plateau region, the 8th-order polynomial achieved the lowest root mean squared error (RMSE) without introducing noticeable overfitting, as verified through cross-validation.

To further refine the coefficients and avoid local minima, a genetic algorithm (GA) was employed. GA hyperparameter was set with a population size of 50, mutation probability of 0.05 and crossover probability of 0.8. The fitness function minimized the mean squared error between measured and estimated OCV values. The algorithm was terminated either after 200 generations or if the fitness improvement remained below 10^{-6} for 20 consecutive generations, whichever occurred first.

The resulting polynomial equation was solved iteratively using the Newton–Raphson (NR) method to obtain SOC from a given V_{oc}. The initial SOC guess is set to 0.5 (50%) which represents a neutral midpoint that improves convergence stability across charge–discharge cycles. A convergence tolerance of 10^{-6} was applied to the residual error, with a maximum of 100 iterations permitted. In practice, the method consistently converged within fewer than 10 iterations for all tested cases.

2.4. Neural Network Model

A NN was employed to estimate the time-varying battery parameters V_{oc}, R_i, R_p and C_p, which are essential for estimating SOC. The model receives terminal voltage V_t and current I_b as input features, and the outputs are the internal parameters used to derive SOC through an OCV–SOC mapping. To train the model, the time-series dataset generated in the previous step was used. The architecture of the ANN is illustrated in Fig. 4. The inputs $x1$ and $x2$ correspond to V_t and I_b, while the outputs $\hat{y}1$, $\hat{y}2$, $\hat{y}3$, and $\hat{y}4$ represent V_{oc}, R_i, R_p and C_p, respectively. The ANN architecture consisted of one input layer with two nodes corresponding to terminal voltage and current, two fully connected hidden layers, and one output layer with four nodes representing outputs V_{oc}, R_i, R_p and C_p. Each hidden layer contained 32 neurons with rectified linear unit (ReLU) activation functions, which provided efficient training and mitigated vanishing gradient issues. The output layer used linear activation to predict continuous parameter values. Model training was performed using the Adam optimizer. The initial learning rate is set to 1×10^{-3} and batch size is set to 128 for 200 training epochs. Early stopping was applied to avoid overfitting, with validation performance monitored during training. The detail of the NN hyperparameters used in this research is shown in Table 2.

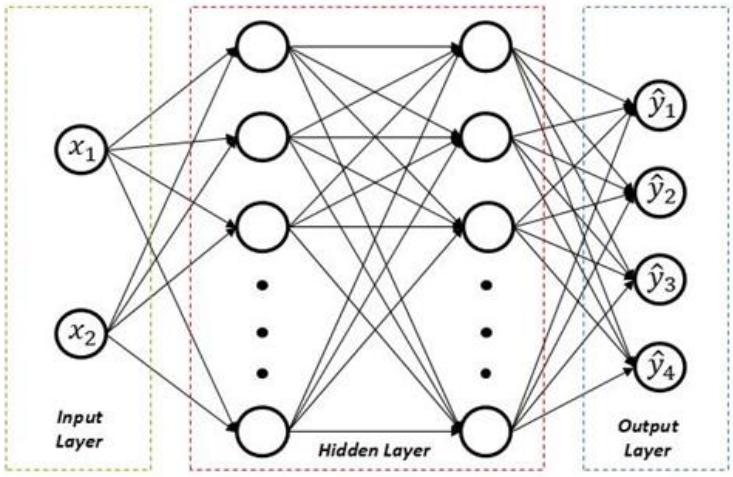

Figure 4. ANN architeture

Table 2. ANN hyperparameters setting

Parameter	Specification
Input layer	2 nodes
Output layer	4 nodes
Hidden layers	2 layers, 32 neurons each
Activation function (hidden layer)	ReLU
Activation function (output layer)	Linear
Batch size	128
Epochs	200 (with early stopping)
Optimizer	Adam
Learning rate	1×10^{-3}

Since this approach incorporates domain knowledge, a PINN framework was implemented. The ANN training is not only aimed to minimize the data training loss but also to comply with the governing physical equations of the Thevenin model. The total loss is a weighted sum of three components:

- Output loss ($\mathcal{L}_{out}$); ensures the predicted terminal voltage matches the measured values.
- RC dynamics constraint ($\mathcal{L}_{RC}$); enforces consistency with the RC branch differential equation.
- SOC consistency loss ($\mathcal{L}_{SOC}$); ensures that the predicted V_{oc} corresponds to SOC using OCV–SOC mapping.

These loss functions are given by:

$$\mathcal{L}_{out} = \frac{1}{N}\sum_{i=1}^{N}\left|V_t(t)_{true} - V_t(t)_{pred}\right|^2 \tag{5}$$

$$\mathcal{L}_{RC} = \frac{1}{N}\sum_{i=1}^{N}\left|\frac{dV_{RC}}{dt} + \frac{1}{R_pC_p}V_{RC} - \frac{0.01}{C_p}\right|^2 \tag{6}$$

$$\mathcal{L}_{SOC} = \frac{1}{N}\sum_{i=1}^{N}\left|SOC(t)_{true} - SOC(t)_{pred}\right|^2 \tag{7}$$

In (12), $SOC(t)_{true}$ is the measured SOC from Coulomb counting, and $SOC(t)_{pred}$ is the corresponding SOC derived from the predicted V_{oc} using the OCV–SOC relation. The total loss is given by:

$$\mathcal{L}_{total} = \alpha.\mathcal{L}_{out} + \beta.\mathcal{L}_{RC} + \gamma.\mathcal{L}_{SOC} \tag{8}$$

Where α, β, and γ are weighting coefficients. In this study, values of α=0.5, β=0.3, and γ=0.2 were selected after preliminary tuning to balance data fidelity, dynamic consistency, and SOC accuracy. This weighting ensures that the model prioritizes accurate reproduction of measured terminal voltage while still enforcing the RC dynamics and SOC consistency constraints. By training under these physics-based constraints, the NN can learn the dynamic behavior of the battery parameters and accurately estimate SOC in real time, ensuring both robustness and physical consistency.

2.5. Model Evaluation

The performance of the proposed PINN in estimating the battery's internal parameters and SOC was assessed using three statistical metrics: root mean square error (RMSE), mean absolute percentage error (MAPE), and the coefficient of determination (R^2). These metrics assess prediction accuracy by

comparing the model's estimated terminal voltage and SOC to the ground truth values. RMSE gives the average size of errors in the same units as the target variable, while MAPE shows the error as a percentage. The R^2 value indicates how well the model captures data variance, with values near 1 suggesting a better fit.

3. Results and Discussion

This section displays the experiment outcomes and the processes of parameter identification, parameter dynamics modeling, and model simulation for real-time SOC estimation of the battery system. The experiment supplied crucial measurement data under varying conditions, and the parameter identification aimed at identifying essential model parameters affecting battery behavior. These parameters were integrated into the model to accurately simulate battery dynamics. The model's efficacy in estimating real-time SOC is assessed via simulation results, detailed in subsequent subsections.

3.1. Parameter Dynamics

The training of the proposed PINN model facilitated the discovery of crucial battery parameters, the main focus of the learning stage. These parameters align with the equivalent circuit model elements, such as the OCV (V_{oc}), polarization voltage (V_p), and internal resistance (R_i). By deriving these from the data, the model precisely models the battery's internal dynamics during charging.

Among these parameters, the OCV (V_{oc}) is crucial as it reliably estimates the SOC. Likewise, the internal resistance (R_i) offers insights into the battery's condition, revealing both immediate response and long-term degradation effects, enhancing SOC estimation accuracy. The polarization voltage (V_p) complements the model by addressing transient voltage behavior from electrochemical processes.

The ability of the model to learn battery behavior was assessed by comparing the estimated values of V_{oc} and R_i. from the training with reference data from experiments. This comparison facilitates an in-depth analysis of the battery system's dynamic response. Fig. 5 presents the estimation results for OCV and internal resistance over the training cycles, showing the ability of the model to accurately capture the dynamics of battery. The findings confirm that this method effectively derives key parameters from voltage-current data during charging, enhancing SOC estimation accuracy and supporting battery health monitoring and reliability.

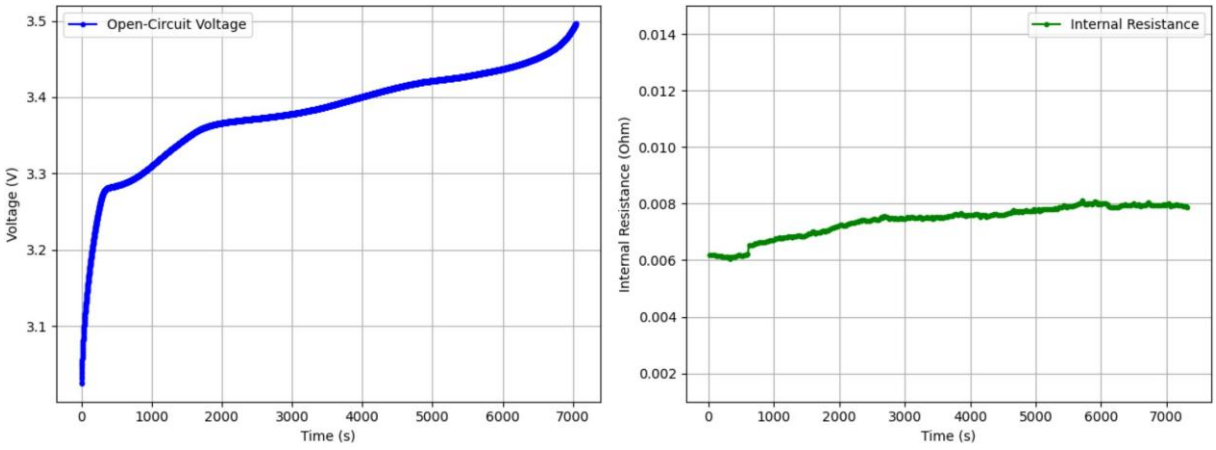

Figure 5. The dynamic estimation of OCV and internal resistance

3.2. OCV-SOC Relationship

As explained in the proposed method, the OCV parameter obtained from NN training is used to estimate SOC of the battery through polynomial regression. As shown in Fig. 5, the estimated OCV has a polynomial relationship with the actual SOC of the battery. Therefore, an eighth-order polynomial regression method is employed to obtain an equation representing the relation between estimated OCV

and actual SOC. To complete equation (4), the values of the coefficients were determined using least square fitting and the result is shown in the following equation:

$$Ocv(SoC) = 2.76 + 5.38\,SOC - 17.28\,SOC^2 + 33.96\,SOC^3 + 2.17\,SOC^4 - 188.17\,SOC^5 + 406.46\,SOC^6 - 350.29\,SOC^7 + 109.6\,SOC^8 \quad (9)$$

Battery SOC can be approached by solving equation (9). To solve it, the NR method was utilized by inputting V_{oc} obtained from PINN training. The initial guess for SOC is set to 0. The SOC prediction result is then compared to the actual SOC obtained from experimental data to validate model accuracy, as shown in Fig. 6.

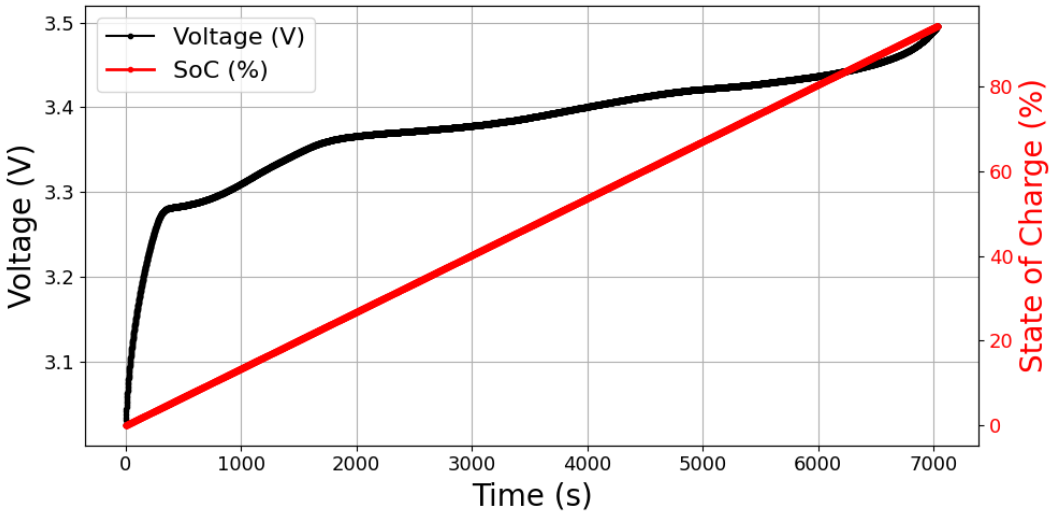

Figure 6. The relationship between actual SOC and estimated open circuit voltage

3.3. Hyperparameter Sensitivity Analysis

Fig. 7 presents the results of the sensitivity analysis for two parameters including the number of hidden layers and the number of neurons per hidden layer. As shown in Neurons vs RMSE sensitivity analysis plot, increasing the number of neurons from very small values initially leads to a sharp reduction in RMSE for both training and testing sets, indicating improved representational capacity of the network. However, beyond about 32 neurons the improvement becomes more gradual, and the curves begin to fluctuate around a lower bound. This suggests that while adding more neurons can enhance model accuracy to some extent, excessive neurons do not necessarily yield further benefits and may even introduce variability due to overfitting.

Meanwhile, Hidden layers vs RMSE sensitivity analysis plot highlights the effect of varying the number of hidden layers. The reduction in RMSE is most significant when moving from a single hidden layer to two layers, confirming that a deeper structure improves the network's ability to capture nonlinearities in the data. Nevertheless, adding more than two layers results in only marginal improvements for training RMSE and even leads to a slight increase in testing RMSE, reflecting reduced generalization and potential overfitting. Taken together, these findings support the selection of a moderate network architecture with two hidden layers and 32 neurons each as a balanced choice between accuracy and robustness.

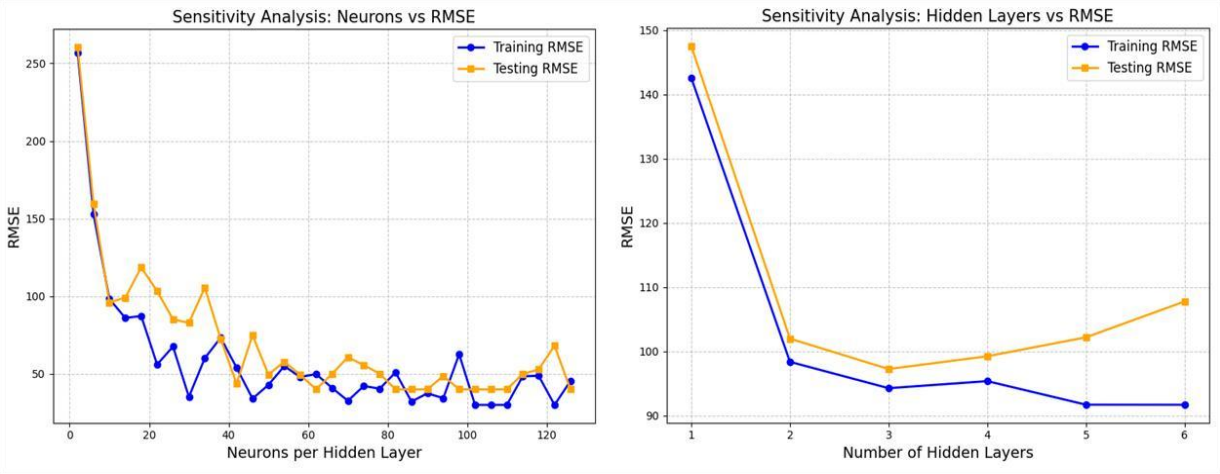

Figure 7. Hyperparameter sensitivity analysis (Hidden layer and neurons)

3.4. SOC Estimation Result

The final SOC estimation result using proposed method is obtained by converting the estimated open circuit voltage value through (9). The obtained SOC estimation value then compared with obtained SOC from experiments using pure NN method and physic-based model with KF as presented in Fig. 8. The actual SOC trajectory, derived from high-resolution experimental data was used as the reference baseline. All estimation curves closely follow the ground truth across the charge cycle, though significant differences emerge in terms of transient behavior and steady-state accuracy.

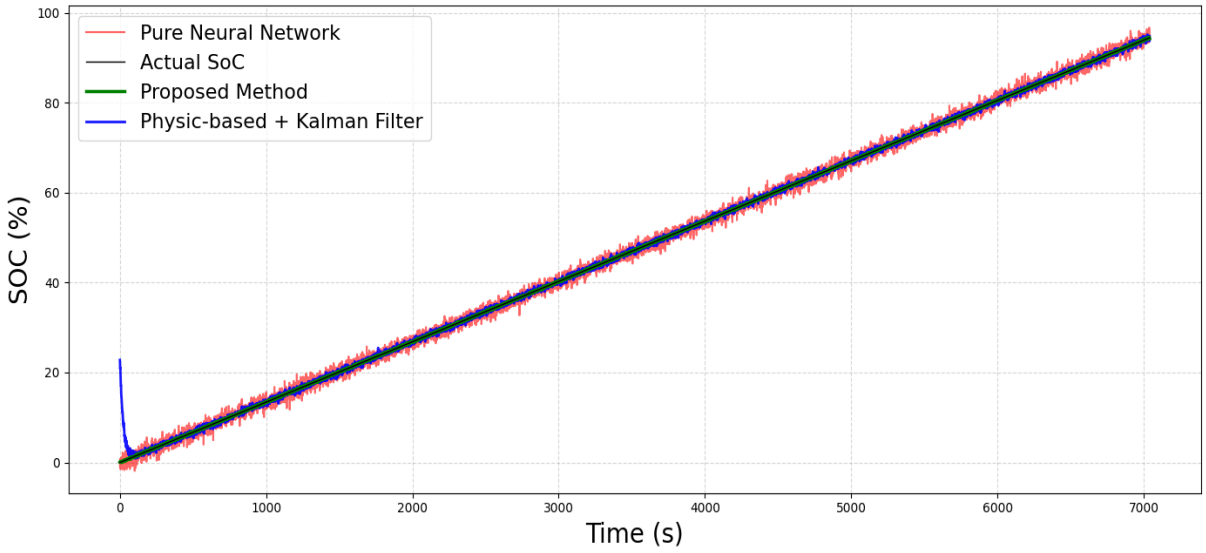

Figure 8. SOC estimation results from various methods

Quantitative evaluation was conducted using three performance metrics including RMSE, MAPE, and R^2. These metrics, summarized in Table 3, reveal that the proposed PINN significantly outperforms the other methods. It achieves the lowest RMSE of 0.103, the smallest MAPE of 0.702%, and the highest R^2 of 0.998. These results indicate both high estimation precision and strong correlation with the ground-truth SOC, underscoring the effectiveness of embedding physical constraints within a neural learning framework.

Table 3. SOC Estimation Error Comparison

Methods	**RMSE**	**MAPE**	R^2
Pure NN	0.703	1.462	0.997
Pure Physic-based Model	1.410	3.377	0.995
Proposed Method	**0.103**	**0.702**	**0.998**

The pure NN baseline demonstrates competitive accuracy, with RMSE of 0.703 and R^2 of 0.997, but the MAPE rises to 1.462%. This higher percentage error is linked to the absence of physical priors that makes the network more prone to noise and overfitting in regions where training data are limited. As a result, its transient predictions become less stable, a well-documented drawback of unconstrained black-box models.

The physics-based model with Kalman filtering provides greater interpretability and noise suppression during steady states, yet it records the largest estimation errors (RMSE = 1.410, MAPE = 3.377%). The reduced R^2 (0.995) indicates weaker tracking during highly nonlinear charge–discharge phases. A key source of error lies in the filter's sensitivity to initial conditions and covariance assumptions, which produced large deviations at the beginning of the estimation horizon. Since the Kalman filter relies on local linearization, it cannot fully capture the strong nonlinearities that dominate under rapid current changes, leading to biased estimates before the filter converges.

The error distribution shown in Fig. 9 provides further insight into these observations. The physics-based method exhibits a wide spread of error values, especially at the beginning of the estimation horizon, confirming its sensitivity to initialization and filter tuning. By contrast, the pure NN baseline produces narrower but more irregular fluctuations, consistent with its tendency to amplify noise in regions lacking sufficient training support. The proposed approach, however, demonstrates the most compact distribution centered closely around zero, indicating both lower bias and reduced variance in its error profile. This visual evidence reinforces the numerical metrics, highlighting that the PINN not only minimizes average error but also stabilizes transient behavior across the entire time horizon.

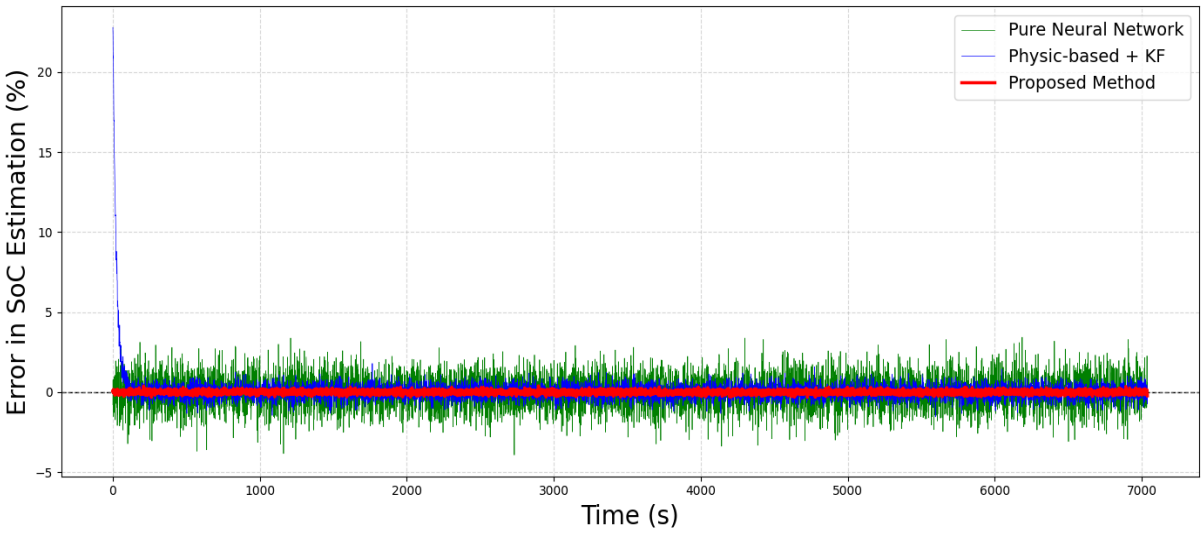

Figure 9. Error distribution plot

In contrast, the proposed PINN integrates the strengths of both approaches. By incorporating differential constraints from the Thevenin model, the PINN reduces sensitivity to noisy or sparse data that typically destabilize pure NN predictions. At the same time, the learning component captures

nonlinear dynamics beyond the reach of linearized Kalman filtering. This hybrid structure explains why the method delivers both low absolute error and smooth transient performance. In effect, the physics priors restrict the hypothesis space, guiding the neural network toward physically consistent solutions, while the data-driven learning ensures adaptability to real operating conditions. This synergy accounts for the observed improvement in accuracy and robustness, particularly during dynamic load transitions where other methods show noticeable limitations.

In addition, the proposed method also shows efficiency in computation. Table 4 summarizes average runtime per cycle and approximate floating-point operations (FLOPs) for the three estimators. From these data, the analysis is derived into two metrics: FLOPs per millisecond and time per FLOP. The pure NN requires the largest number of arithmetic operations (8.02×10^4 FLOPs) and the longest average latency (7.8 ms), but exhibits the lowest time per FLOP (≈97 ns/FLOP), indicating that its arithmetic workload is highly vectorizable and benefits from optimized dense linear algebra kernels. The pure physic-based model has very low computational complexity (1.5×10^3 FLOPs) and the smallest total runtime (3.2 ms), yet shows the highest time per FLOP (≈2,133 ns/FLOP), which suggests that its wall-time is dominated by non-FLOP overheads (control branching, scalar operations, or interpreter overhead). The proposed PINN achieves an intermediate computational cost (1.2×10^4 FLOPs) and latency (5.1 ms), reflecting its mixed character (neural inference plus modest physics processing).

Table 4. Computational complexity comparison

Methods	Average runtime per cycle (ms)	Approximated FLOPs per cycle
Pure NN	7.8	8.02×10^4
Pure Physic-based Model	3.2	1.5×10^3
Proposed Method	**5.1**	$\mathbf{1.2 \times 10^4}$

The comparison shows that the proposed method offers the most balanced trade between the accuracy and the cost of computation. Relative to the pure physics-based model, the method requires additional computation because of the neural network component, but the increase is modest and outweighed by the significant improvement in accuracy. In contrast, compared with a purely data-driven NN, the proposed method achieves both higher accuracy and lower computational demand. This outcome arises from the hybrid design: the equivalent circuit model restricts the solution space with physically grounded constraints, while the neural network captures nonlinear dynamics that are difficult to express analytically. By embedding physical structure into the learning process, the network can remain compact without sacrificing performance. Consequently, the method delivers markedly higher accuracy while keeping runtime within practical limits for real-time battery management applications.

The findings emphasize the strength of combining data-driven learning with physical modeling. Because the PINN enforces differential constraints and system dynamics, it can maintain accurate SOC estimation across the full operating range. This shows that physics-informed learning is particularly valuable in safety-critical settings, where accuracy must be accompanied by interpretability. Unlike black-box neural networks, the proposed framework offers greater confidence in prediction reliability by remaining consistent with established battery behaviors.

These benefits also extend to practical use in battery management systems. In electric vehicles, more accurate SOC estimation means drivers can rely on improved range prediction, longer usable driving distance, and better safeguards against overcharge or deep discharge. For large battery energy storage systems, the method's robustness under variable loads and repeated cycling helps ensure stable grid operation and dependable renewable energy dispatch. Although the computational cost of the PINN is higher than a purely physics-based model, it remains well within the limits of common embedded controllers used in automotive and stationary BMS. This balance of accuracy and efficiency makes the approach not only technically sound but also realistically deployable.

While the proposed PINN demonstrates clear advantages, certain limitations should be acknowledged. The experiment was conducted under a fixed temperature of 20 °C and with predefined charge–discharge rates. As a result, the generalization of the model across a broader temperature range or under highly variable C-rates has not yet been validated. In practical BMS applications, thermal effects and current-rate fluctuations strongly influence internal battery dynamics, and further testing is required to confirm robustness under such conditions. Moreover, this study only focuses on $LiFePO_4$ cells, and the applicability of the framework to other chemistries such as NMC or LCO remains an open question. Differences in OCV–SOC characteristics and degradation pathways may require re-tuning of the polynomial fitting or additional modifications to the loss formulation. These aspects point to the need for future work on transferability and cross-chemistry adaptation before large-scale deployment in diverse battery systems.

4. Conclusion

A novel method for real-time SOC estimation of lithium-ion batteries using a dynamic model with a PINN has been successfully developed. This approach blends experimental data with internal battery dynamics such as polarization voltage, OCV, and internal resistance. Parameter values were initially obtained from an equivalent circuit model, and behavior dynamics were learned via PINN training, facilitating accurate SOC tracking. The OCV-SOC relationship was modeled using an eighth-order polynomial regression, with coefficients optimized via a GA. The final SOC estimates were obtained using the NR method and validated against experimental data. Comparative analysis showed that the proposed PINN method outperformed both pure NN and physics-based models with Kalman filters, achieving the lowest RMSE (0.103), MAPE (0.702%), and highest R^2 (0.998). These results confirm the effectiveness of embedding physic-based knowledge into the NN training. The PINN approach improves robustness, accuracy, and interpretability in dynamic and nonlinear conditions. This hybrid model was shown to improve robustness, accuracy, and interpretability. Despite its strong performance, this study is limited to $LiFePO_4$ cells tested under fixed laboratory conditions. Broader validation across temperatures, C-rates, and chemistries is required. Future work will incorporate thermal coupling, integrate SOH estimation, and evaluate deployment on embedded BMS hardware. With these extensions, the proposed PINN can further enhance the safety and reliability of EV or energy storage systems.

Acknowledgements

The authors are grateful to the Universitas Sebelas Maret as this work was funded through Penelitian Fundamental A (PFA-UNS) research grant with contract number 369/UN27.22/PT.01.03/2025.

References

[1] Adaikkappan A, Maheshwari M, Sathiyamoorthy N. Modeling, state of charge estimation, and charging of lithium-ion battery in electric vehicle: a review. Int J Energy Res 2022;46(3):2141–65. https://doi.org/10.1002/er.7339.

[2] Apribowo CHB, Hadi SP, Wijaya FD, Sarjiya. Optimal sizing and siting of fresh and second-life battery energy storage systems based on linearized optimal power flow for high photovoltaic penetration: A comparative study. Evergreen 2024;11(3):2202–16. https://doi.org/10.5109/7236864.

[3] Apribowo CHB, Sarjiya, Hadi SP, Wijaya FD. Integration of battery energy storage system to increase flexibility and penetration of renewable energy in Indonesia: A brief review. In: Proceedings of the International Conference on Power and Energy. IEEE; 2022. https://doi.org/10.1109/ICPERE56870.2022.10037530 .

[4] Tian J, Xiong R, Lu J, Chen C, Shen W. Battery state-of-charge estimation amid dynamic usage with physics-informed deep learning. Energy Storage Mater 2022;50:718–29. https://doi.org/10.1016/j.ensm.2022.12.020.

[5] Xu Z, Wang J, Lund PD, Zhang Y. Co-estimating the state of charge and health of lithium

batteries through combining a minimalist electrochemical model and an equivalent circuit model. Energy 2022;240:122815. https://doi.org/10.1016/j.energy.2021.122815.
[6] Gao Y, Liu K, Zhu C, Zhang X, Zhang D. Co-estimation of state-of-charge and state-of-health for lithium-ion batteries using an enhanced electrochemical model. IEEE Trans Ind Electron 2021;69(3):2684–96. https://doi.org/10.1109/TIE.2021.3066946.
[7] Tao Z, Zhao Z, Wang C, Huang L, Jie H, Li H, Hao Q, Zhou Y, See KY. State of charge estimation of lithium batteries: Review for equivalent circuit model methods. Measurement 2024;236:115148. https://doi.org/10.1016/j.measurement.2023.115148.
[8] Thakkar RR. Electrical equivalent circuit models of lithium-ion battery. In: Management and Applications of Energy Storage Devices. IntechOpen; 2021. https://doi.org/10.5772/intechopen.99851.
[9] Salazar D, Garcia M. Estimation and comparison of SOC in batteries used in electromobility using the Thevenin model and coulomb ampere counting. Energies 2022;15(19):7204. https://doi.org/10.3390/en15197204.
[10] Pande AS, Soni BP, Bhadane KV. Electrical models for EV's batteries: an overview and mathematical design of RC network. J Inst Eng (India) Ser B 2023;104(2):533–47. https://doi.org/10.1007/s40031-022-00852-1.
[11] Apribowo CHB, Hadi SP, Wijaya FD, et al. Optimal sizing and siting of battery energy storage systems with retired battery. In: 2022 International Conference on Technology and Policy in Energy and Electric Power (ICT-PEP). Piscataway (NJ): IEEE; 2022. p. 327–32. https://doi.org/10.1109/ICT-PEP57242.2022.9988958.
[12] Lucaferri V, Quercio M, Laudani A, Riganti Fulginei F. A review on battery model-based and data-driven methods for battery management systems. Energies 2023;16(23):7807. https://doi.org/10.3390/en16237807.
[13] Priya R, Purnima R, Sakile R. State of charge estimation of lithium-ion battery based on extended Kalman filter and unscented Kalman filter techniques. Energy Storage 2023;5(3):e408. https://doi.org/10.1002/est2.408.
[14] Hossain M, Haque ME, Arif MT. Kalman filtering techniques for the online model parameters and state of charge estimation of the Li-ion batteries: A comparative analysis. J Energy Storage 2022;51:104174. https://doi.org/10.1016/j.est.2022.104174.
[15] Zepka R, Bischof S, Blank T. Implementing an extended Kalman filter for SOC estimation of a Li-ion battery with hysteresis: A step-by-step guide. Energies 2021;14(13):3733. https://doi.org/10.3390/en14133733.
[16] Liu X, Qiule L, Li W, Mingqiang L, Ji W. Data-driven state of charge estimation for power battery with improved extended Kalman filter. IEEE Trans Instrum Meas 2023;72:1–10. https://doi.org/10.1109/TIM.2023.3239629.
[17] Zhang S, Chen Z, Shiyong J, Xiongwen Z. A comparative study of different adaptive extended/unscented Kalman filters for lithium-ion battery state-of-charge estimation. Energy 2022;246:123423. https://doi.org/10.1016/j.energy.2022.123423.
[18] Hossain M, Enamul HMD, Arif MT. Online model parameter and state of charge estimation of Li-ion battery using unscented Kalman filter considering effects of temperatures and C-rates. IEEE Trans Energy Convers 2022;37(4):2498–511. https://doi.org/10.1109/TEC.2022.3178600.
[19] Wang S, Jia X, Takyi-Aninakwa P, Stroe DI, Fernandez C. Optimized particle filtering strategies for high-accuracy state of charge estimation of LIBs. J Electrochem Soc 2023;170(5):050514. https://doi.org/10.1149/1945-7111/acd148.
[20] Zhang C, Zhao H, Wang L, Liao C, Wang L. A comparative study on state-of-charge estimation for lithium-rich manganese-based battery based on Bayesian filtering and machine learning methods. Energy 2024;306:132349. https://doi.org/10.1016/j.energy.2024.132349.
[21] Sesidhar DVSR, Badachi C, Green RC. A review on data-driven SOC estimation with Li-ion batteries: Implementation methods and future aspirations. J Energy Storage 2023;72:108420. https://doi.org/10.1016/j.est.2023.108420.

[22] Lipu MH, Hannan MA, Aini H, Shaheer A, Rahman SA, Mohamad HM, Kashem MM. Real-time state of charge estimation of lithium-ion batteries using optimized random forest regression algorithm. IEEE Trans Intell Veh 2022;8(1):639–48. https://doi.org/10.1109/TIV.2022.3161301.
[23] Jafari S, Yang JH, Byun YC. Optimized XGBoost modeling for accurate battery capacity degradation prediction. Results Eng 2024;24:102786. https://doi.org/10.1016/j.rineng.2024.102786.
[24] Tian J, Chen C, Shen W, Sun F, Xiong R. Deep learning framework for lithium-ion battery state of charge estimation: Recent advances and future perspectives. Energy Storage Mater 2023;61:102883. https://doi.org/10.1016/j.ensm.2023.102883.
[25] Guo S, Ma L. A comparative study of different deep learning algorithms for lithium-ion batteries on state-of-charge estimation. Energy 2023;263:125872. https://doi.org/10.1016/j.energy.2022.125872.
[26] Fan X, Zhang W, Zhang C, Chen A, An F. SOC estimation of Li-ion battery using convolutional neural network with U-Net architecture. Energy 2022;256:124612. https://doi.org/10.1016/j.energy.2022.124612.
[27] Chen J, Zhang Y, Wu J, Cheng W, Zhu Q. SOC estimation for lithium-ion battery using the LSTM-RNN with extended input and constrained output. Energy 2023;262:125375. https://doi.org/10.1016/j.energy.2022.125375.
[28] Zhao Y, Li Y, Cao Y, Jiang L, Wan J, Rehtanz C. An RNN with small sequence trained by multi-level optimization for SOC estimation in Li-ion battery applications. IEEE Trans Veh Technol 2023;72(9):11469–81. https://doi.org/10.1109/TVT.2023.3267500.
[29] Cui Z, Wang L, Li Q, Wang K. A comprehensive review on the state of charge estimation for lithium-ion battery based on neural network. Int J Energy Res 2022;46(5):5423–40. https://doi.org/10.1002/er.7545.
[30] Chai X, Shihao L, Liang F. A novel battery SOC estimation method based on random search optimized LSTM neural network. Energy 2024;306:132583. https://doi.org/10.1016/j.energy.2024.132583.
[31] Wu Y, Bai D, Zhang K, Li Y, Yang F. Advancements in the estimation of the state of charge of lithium-ion battery: A comprehensive review of traditional and deep learning approaches. J Mater Inform 2025;5(2). https://doi.org/10.20517/jmi.2024.84.
[32] Yi Y, Xia C, Shi L, Meng L, Chi Q, Qian L, Ma T, Chen S. Lithium-ion battery expansion mechanism and Gaussian process regression based state of charge estimation with expansion characteristics. Energy 2024;292:130541. https://doi.org/10.1016/j.energy.2024.130541.
[33] Apribowo CH, Dyartanti ER, Al Farisi S, Hafidzsyah H. Design and development of battery cell protection system on LFP battery pack using bypass techniques. In: 2023 International Conference on Technology and Policy in Energy and Electric Power (ICT-PEP). IEEE; 2023. p. 316–21. https://doi.org/10.1109/ICT-PEP60152.2023.10351176.
[34] Mehta C, Sant AV, Sharma P. SVM-assisted ANN model with principal component analysis based dimensionality reduction for enhancing state-of-charge estimation in LiFePO4 batteries. e-Prime Adv Electr Eng Electron Energy 2024;8:100596. https://doi.org/10.1016/j.prime.2024.10059.
[35] Zhang G, Xia B, Wang J, Ye B, Chen Y, Yu Z, Li Y. Intelligent state of charge estimation of battery pack based on particle swarm optimization algorithm improved radial basis function neural network. J Energy Storage 2022;50:104211. https://doi.org/10.1016/j.est.2022.104211.
[36] Singh S, Ebongue YE, Rezaei S, Birke KP. Hybrid modeling of lithium-ion battery: Physics-informed neural network for battery state estimation. Batteries 2023;9(6):301. https://doi.org/10.3390/batteries9060301.
[37] Navidi S, Thelen A, Li T, Hu C. Physics-informed machine learning for battery degradation diagnostics: A comparison of state-of-the-art methods. Energy Storage Mater 2024;68:103343. https://doi.org/10.1016/j.ensm.2024.103343.
[38] Dezhi S, Ding J, Hao T. Elman neural network and Thevenin equivalent circuit model based

multi-measurement Kalman filter for SOC estimation. Ionics 2024;30(2):833–45. https://doi.org/10.1007/s11581-023-05307-1.
[39] Wang Q, Min Y, Bin L, Gaoqi L, Yan L. Co-estimation of state of charge and capacity for battery packs in real electric vehicles with few representative cells and physics-informed machine learning. Energy 2024;306:132520. https://doi.org/10.1016/j.energy.2024.132520.
[40] Su S, Wei L, Jianhui M, Akhil G, Liang G, Jie L. A hybrid battery equivalent circuit model, deep learning, and transfer learning for battery state monitoring. IEEE Trans Transp Electrif 2022;9(1):1113–27. https://doi.org/10.1109/TTE.2022.3204843.
[41] Dang L, Yang J, Liu M, Chen. Differential equation-informed neural network for state-of-charge estimation. IEEE Trans Instrum Meas 2023;73:1–5. https://doi.org/10.1109/TIM.2023.3334377.
[42] Gao Y, Plett GL, Fan G, Zhang X. Enhanced state-of-charge estimation of LiFePO4 batteries using an augmented physics-based model. J Power Sources 2022;544:231889. https://doi.org/10.1016/j.jpowsour.2022.231889.